Secondary Structure and Lipid Contact of a Peptide Antibiotic in Phospholipid Bilayers by REDOR

Orsolya Toke,* W. Lee Maloy,† Sung Joon Kim,‡ Jack Blazyk,§ and Jacob Schaefer*
*Department of Chemistry, Washington University, St. Louis, Missouri 63130; †Genaera Pharmaceuticals, Plymouth Meeting, Pennsylvania 19462; ‡Department of Molecular Biophysics, Washington University School of Medicine, St. Louis, Missouri 63130; §Department of Biomedical Sciences, College of Osteopathic Medicine and Department of Chemistry and Biochemistry, College of Arts and Sciences, Ohio University, Athens, Ohio 45701

ABSTRACT The chemical shifts of specific ^{13}C and ^{15}N labels distributed throughout KIAGKIA-KIAGKIA-KIAGKIA (K3), an amphiphilic 21-residue antimicrobial peptide, prove that the peptide is in an all α-helical conformation in the bilayers of multilamellar vesicles (MLVs) containing dipalmitoylphosphatidylcholine and dipalmitoylphosphatidylglycerol (1:1). Rotational-echo double-resonance (REDOR) $^{13}C\{^{31}P\}$ and $^{15}N\{^{31}P\}$ experiments on the same labeled MLVs show that on partitioning into the bilayer, the peptide chains remain in contact with lipid headgroups. The amphipathic lysine side chains of K3 in particular appear to play a key role in the electrostatic interactions with the acidic lipid headgroups. In addition to the extensive peptide-headgroup contact, $^{13}C\{^{19}F\}$ REDOR experiments on MLVs containing specifically ^{19}F-labeled lipid tails suggest that a portion of the peptide is surrounded by a large number of lipid acyl chains. Complementary $^{31}P\{^{19}F\}$ REDOR experiments on these MLVs show an enhanced headgroup-lipid tail contact resulting from the presence of K3. Despite these distortions, static ^{31}P NMR lineshapes indicate that the lamellar structure of the membrane is preserved.

INTRODUCTION

Peptide antibiotics

Magainins are amphiphilic peptides with a wide range of antimicrobial activity (Matsuzaki, 1998a; Huang, 2000). They were first isolated from the African clawed frog, *Xenopus laevis* (Zasloff, 1987). Similar to other antimicrobial peptides (Andreu and Rivas, 1998; Epand and Vogel, 1999; Hancock and Diamond, 2000; van't Hof et al., 2001), magainins are thought to form some sort of an ion channel or pore in bacterial membranes, thereby enhancing the ion permeability of the membrane and destroying the cell (Bowman et al., 1994; Matsuzaki, 1998b). However, the mechanism of pore formation is poorly understood and even the secondary structure of the peptides in the membrane is a subject of continuing debate (Bechinger et al., 1993; Hirsh et al., 1996).

$(KIAGKIA)_3$-NH_2 (K3) (Maloy and Kari, 1995) is a synthetic analog of PGLa (Soravia et al., 1988), an antimicrobial magainin-like peptide also found in the skin secretions of *Xenopus laevis*. Recently it has been shown that upon partitioning into membranes, K3 adopts primarily an α-helical conformation (Blazyk et al., 2001). The sequence of K3 contains three repeats of a heptamer, KIAGKIA-KIAGKIA-KIAGKIA, giving rise to a highly positively charged, amphipathic peptide chain. K3 exhibits higher activity against both Gram-negative and Gram-positive bacteria (Maloy and Kari, 1995) than any of the currently known natural *Xenopus* peptides, including the widely studied magainins (Zasloff, 1987; Matsuzaki, 1998a,b; Huang 2000), yet it retains low activity against eukaryotic cells.

The mode of action of K3 could involve any of a variety of general mechanisms that have been proposed for peptide antibiotics. One possibility (Fig. 1 *A*) is that the peptide aggregates on the surface of the membrane and then inserts into the bilayer forming a so-called barrel-stave pore (Ehrenstein and Lecar, 1977). Another possibility (Fig. 1 *B*) is that the accumulation of peptide on the membrane surface forms a destabilizing carpet, leading to a local disintegration of the bilayer (Pouny et al., 1992). A third possibility (Fig. 1 *C*) is that peptide chains aggregate on the membrane surface, possibly forming a carpet (Shai, 1999), partially submerge, and then blend with lipids so that peptide chains and lipid headgroups together line the wall of a toroidal pore (Huang, 2000). In this scheme, the phospholipid headgroups have an important role in screening the electrostatic repulsions between the highly positively charged peptide chains. Headgroup incorporation into the pore allows substantially larger pore sizes (Ludtke et al., 1996) than the barrel-stave pore model (Fig. 1).

Solid-state NMR

In this article (I) and the following companion article (II), we report the use of solid-state NMR to distinguish between the three models of Fig. 1 for K3 in bilayers. In the experiments described in I, specific ^{13}C and ^{15}N labels were introduced into K3 so that isotropic chemical shifts accurately reveal its local secondary structure at the middle and near both ends of

Submitted August 5, 2003, and accepted for publication March 4, 2004.

Address reprint requests to Jacob Schaefer, Dept. of Chemistry, Washington University, 1 Brookings Dr., St. Louis, MO 63130. Tel.: 314-935-6844; Fax: 314-935-4481; E-mail: schaefer@wuchem.wustl.edu

0006-3495/04/07/662/13 $2.00

doi: 10.1529/biophysj.103.032706

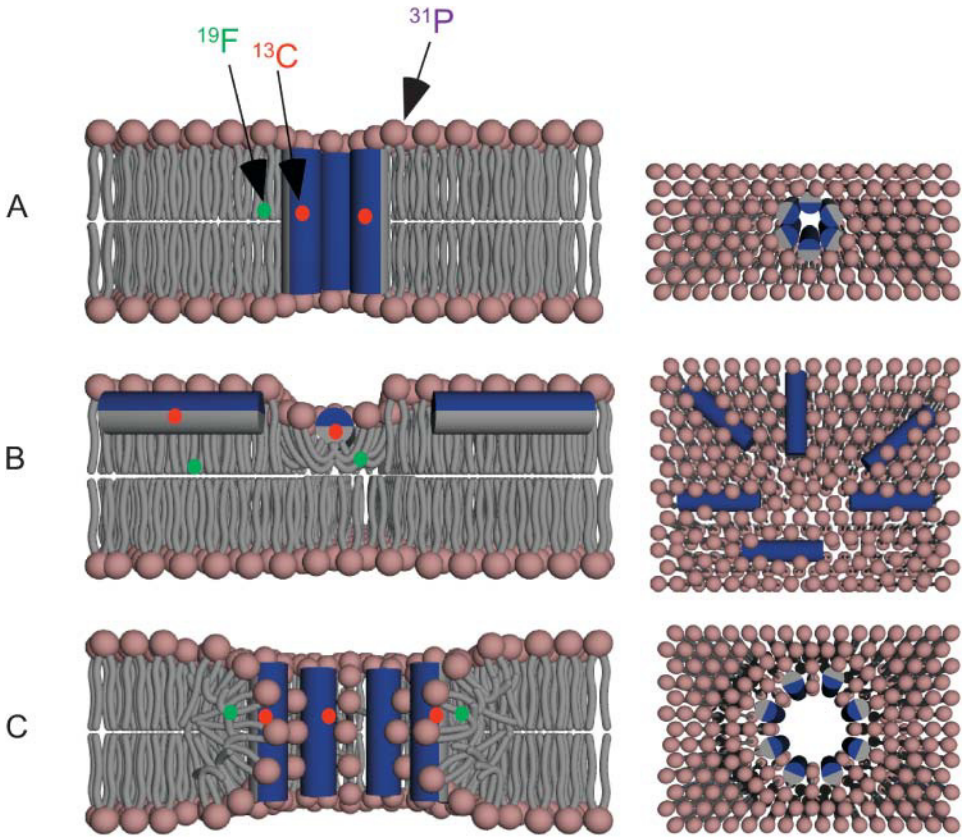

FIGURE 1 Cartoons of various pore models of α-helical antimicrobial peptides: (*A*) barrel-stave, (*B*) carpet, and (*C*) toroid. The hydrophilic and hydrophobic faces of the peptides (shown as cylinders) are colored in blue and gray, respectively. Incorporation of site-specific ^{13}C (*red*) and ^{19}F (*green*) labels into the peptide as well as the lipid acyl chains, allows monitoring peptide-headgroup as well as peptide-lipid tail contacts in the bilayer, thereby distinguishing between the models.

the peptide. In addition, the proximities of these labels to ^{31}P and ^{19}F incorporated in the lipids establish the positioning of K3 relative to the phospholipid headgroups and tails. The spatial proximities between labels are determined by heteronuclear dipolar couplings, which are measured by rotational-echo double resonance (REDOR) (Gullion and Schaefer, 1989ab). These proximities differ significantly for the three models (see Fig. 1). In the experiments described in II, different sets of labels were inserted into K3 so that the heteronuclear dipolar couplings now reveal chain aggregation and orientation directly.

The REDOR NMR sample

A complication in the use of dipolar couplings to determine proximities of labels in bilayers is that the couplings are reduced by motional averaging. Thus, weak couplings associated with internuclear distances of 10 Å or more between lipids and peptides in membrane bilayers at 37°C simply cannot be determined by the available REDOR technology. The solution to this problem is to freeze the bilayer to stop all large-amplitude motions. Unfortunately, biophysically important details of the lipid structure that depend on dynamics are lost by freezing. Nevertheless, the qualitative organizational features of K3 in a bilayer (in particular, peptide conformation and relative proximities to lipid headgroups), which are important to distinguish between the three models of Fig. 1, are not substantively changed by freezing.

Although dipolar couplings can now be determined by REDOR performed on frozen suspensions of multilamellar vesicles (MLVs), the sensitivity of the experiment is compromised by a poor filling factor. Most of the sample is still water. This means that accurate weak-coupling determinations of peptide-peptide separation and orientation, for example, are difficult. The solution to this problem is to lyophilize the sample to remove the nonstructural water. The lyophilization is done in the presence of sugar lyoprotectants to preserve important hydrogen bonds (Crowe and Crowe, 1984; Rudolph and Crowe, 1985).

The lyophilized MLVs are not completely dehydrated (we have detected 15% w/w water), but a lyophilized MLV sample is nevertheless not suitable for a rigorous determination of lipid structure. Thus, the quantitative details of lipid headgroup distortions and lipid-tail disorder, which are observed in lyophilized MLVs with and without K3, will largely be ignored in distinguishing between the three models of Fig. 1 for K3 in bilayers. In addition, it is possible that lyophilization has affected peptide aggregation. However, tightly packed large aggregates are not found in the lyophilized MLVs (II), so they certainly are not present in fully hydrated MLVs. Moreover, the small tightly packed

peptide aggregates that are found (at high resolution) in lyophilized MLVs are also found (at low resolution) in fully hydrated vesicles (II). Thus, it seems reasonable to accept the high-resolution characterization of the aggregates (in particular, the determination of size and internal structure) as biophysically relevant.

MATERIALS AND METHODS

Peptide synthesis and purification

Peptides were synthesized by Genaera Pharmaceuticals (Plymouth Meeting, PA) on an Applied Biosystems model 431A peptide synthesizer. [3-^{13}C]Ala_3-[^{15}N]Gly_4-[1-^{13}C]Ala_{10}-[2-^{13}C]Gly_{11}-[6-^{15}N]Lys_{12}-[1-^{13}C]Ala_{17}-[^{15}N]Gly_{18}-$(KIAGKIA)_3$-NH_2 (MSI-1711), [1-^{13}C]Ala_{10}-[^{15}N]Gly_{11}-$(KIAGKIA)_3$-NH_2 (MSI-1245), and [2-^{2}H, 3-^{19}F]Ala_{10}-$(KIAGKIA)_3$-NH_2 (MSI-1516) were synthesized using regular F-moc (*N*-9-fluorenyl)methoxycarbonyl) chemistry and isotopically labeled amino acids. MSI-1711 and MSI-1245 were cleaved from the resin using trifluoroacetic acid, whereas in the case of MSI-1516 hydrofluoric acid was used. The crude peptides were purified by reverse-phase high-performance liquid chromatography (HPLC) and lyophilized. Purity was confirmed by analytical HPLC and electrospray mass spectrometry by Genaera Pharmaceuticals.

Because some of our NMR experiments required site-specific ^{19}F labels, the peptides had to be further purified to remove fluorinated solvent. This was done using a Poly CAT A low-pressure ion-exchange column (Western Analytical Products, Murrieta, CA). Briefly, the peptides were dissolved in deionized water and neutralized to pH = 7.0 by dropwise addition of 0.1 N NH_4OH and loaded on a Poly CAT A column (7.2mm × 26mm) preequilibrated with 10 mM NH_4OAc, 20% acetonitrile (buffer A). After washing with four column volumes of buffer A, the peptide was eluated with buffer A plus 20% acetic acid; 2-mL fractions were collected and analyzed on analytical HPLC. Acetonitrile was rotoevaporated before lyophilization. Purity was checked by electrospray mass spectrometry and solution NMR spectroscopy. Peptides were stored at −20°C.

Synthesis of 16-fluoropalmitic acid and F-DPPG/F-DPPC

16-Fluoropalmitic acid was synthesized from 16-hydroxypalmitic acid (Aldrich Chemical, Milwaukee, WI) using diethylaminosulfur trifluoride (Esfahani et al., 1981). The final product was purified by flash chromatography to give 90–95% of the acid as a white solid. The fluorolipids 1-palmitoyl-2-[16-fluoropalmitoyl]-phosphatidylcholine (F-DPPC) and 1-palmitoyl-2-[16-fluoropalmitoyl]-phosphatidylglycerol (F-DPPG) were synthesized from 16-fluoropalmitic acid by Avanti Polar Lipids (Alabaster, AL) using lysopalmitoylphosphatidylcholine or lysopalmitoylphosphatidylglycerol to form F-DPPC or F-DPPG, respectively.

Vesicle preparation

Lyophilized samples

A 1:1 molar mixture of dipalmitoylphosphatidylcholine (DPPC) and dipalmitoylphosphatidylglycerol (DPPG) (Avanti Polar Lipids) was dissolved in $CHCl_3$/MeOH (2:1, v/v) to ensure thorough mixing. For fluorinated vesicle preparations, 2.5 or 5.0 mol % of F-DPPC and F-DPPG were incorporated on an equimolar basis into the lipid mixture. The solvent was removed under dry N_2 at 37°C followed by storage under vacuum overnight. The peptide was dissolved in buffer (20 mM piperazine-*N*,*N*′-bis(2-ethanesulfonic acid (PIPES), 1 mM EDTA (pH 7.0)) at room temperature. The dried lipids were resuspended in the peptide-containing buffer at 65°C to give the desired lipid/peptide molar ratio (L/P). For lyoprotection, an amount of trehalose equivalent to 20% of the dry weight of the phospholipids was also incorporated (Crowe and Crowe, 1984; Rudolph and Crowe, 1985). The resulting suspension was subjected to five cycles of freezing (dry ice/EtOH), warming to $T = 65°C > T_m$, (where T_m is the phase transition temperature of the phospholipids), and mixing with a vortex mixer. The sample was lyophilized overnight and then packed into a 7.5-mm outside-diameter zirconia rotor, fitted with plastic (Kel-F) end caps and spacers.

Hydrated samples

Phospholipids were mixed and dried in the same manner as for the lyophilized sample. The dried lipid was resuspended in the peptide-containing buffer (20 mM PIPES, 1 mM EDTA (pH 7.0), lipid/buffer 1:2, w/w) at 65°C to give the desired lipid/peptide molar ratio. The suspension was kept in a 65°C water bath for 5 h with occasional vortex mixing. The sample was cooled to room temperature and packed into a zirconia rotor.

NMR spectroscopy

Experiments were performed using a 4.7-T wide-bore Oxford magnet (Oxford Magnet Technology, Eynsham, UK). The pulse generator and acquisition system were from Tecmag (Houston, TX). Data acquisition was performed with four-channel, transmission-line probes (J. Schaefer and R. A. McKay, 1999. Multi-tuned single-coil transmission-line probe for NMR spectrometer. U.S. Patent No. 5,861,748.). The magic-angle spinning (MAS) modules were from Varian/Chemagnetics (Fort Collins, CO). Carbon-13 free-induction decays were acquired at a controlled MAS speed of 5000 Hz with a recycle delay of 2 s, a ^{1}H decoupling field of 90 kHz, and were processed with a Gaussian line broadening of 80 Hz, unless noted otherwise. Matched spin-locked cross-polarization transfers were performed at 50 kHz with a contact time of 1 ms. Carbon-13 spectra were referenced to the signal from the ^{13}C label of L-[1-^{13}C, 4-^{15}N]asparagine set to 175.1 ppm. This external standard was in turn referenced to tetramethylsilane at 0.0 ppm. The acquisition temperature was ~−10°C for lyophilized samples and −25°C for hydrated frozen samples.

REDOR was done in two parts, once with rotor-synchronized dephasing pulses (S) and once without (S_0). The dephasing pulses change the sign of the heteronuclear dipolar coupling, and this interferes with the spatial averaging resulting from the motion of the rotor (Gullion and Schaefer, 1989a,b). The difference in signal intensity ($\Delta S = S_0 - S$) for the observed spin is directly related to the corresponding distance to the dephasing spin. All π-pulse widths were 10 μs and the XY-8 pulse phase cycling scheme (Gullion et al., 1990) was used to suppress the effects of offsets and pulse imperfections. Homonuclear ^{13}C-^{13}C recoupling was achieved using controlled excitation for dephasing rotational amplitudes (CEDRA), a scheme analogous to REDOR, in which rotor-synchronized π-pulses are used to prevent refocusing of homonuclear dipolar coupling (Zhu et al., 1994). Coherence transfers were made from ^{15}N to ^{13}C by transferred-echo double resonance, a heteronuclear recoupling technique that is useful to eliminate complications from the natural-abundance ^{13}C background (Hing et al., 1992).

Calculation of REDOR dephasing

Dephasing was calculated using a Bessel function expressions for a spin-1/2 pair (Mueller, 1995). This expression was summed over a Gaussian distribution of dipolar couplings corresponding to a distribution of isolated spin pairs. The effects of orientation and averaging for motion of the ^{19}F about the methyl C_3 axis were ignored. This is a reasonable approximation for long-range distances to the CH_2F group (O'Connor et al., 2002). The parameters of the distribution (mean and width) and the overall scaling were varied to minimize the root mean-square deviation between experimental and calculated dephasing (O'Connor and Schaefer, 2002; O'Connor et al., 2002).

RESULTS

Secondary structure of K3 in the lipid bilayer

REDOR spectra after 48 rotor cycles of dipolar evolution of the specifically $^{13}C/^{15}N$ labeled K3 embedded in the MLVs of DPPG/DPPC (1:1) at a lipid/peptide molar ratio of 10 are shown in Fig. 2, with the $^{13}C\{^{15}N\}$ REDOR difference (ΔS) at the top, and the full echo (S_0) at the bottom. Because ^{15}N labels are only in the peptide, the two peaks in the ΔS spectrum are exclusively from the peptide methyl and carbonyl carbons. The main contribution to the methyl peak at 16 ppm is from [3-^{13}C]Ala$_3$. A signal from the natural-abundance ^{13}C in the methyl carbons of Ala$_{17}$ is also present, but is two orders of magnitude smaller than that of the label of Ala$_3$ and can be ignored. The natural-abundance ^{13}C in the methyl carbon of Ala$_{10}$ is not close enough to the [^{15}N]Lys$_{12}$ to contribute to the ΔS spectrum.

The carbonyl-carbon signal that appears in the REDOR difference spectrum of Fig. 2 is predominantly from [1-^{13}C]Ala$_{17}$, but also contains contributions from three natural-abundance carbonyl ^{13}C spins that are one (Ala$_3$) and two (Gly$_4$, Gly$_{18}$) bonds removed from the ^{15}Ns of Gly$_4$ and Gly$_{18}$. The carbonyl-^{13}C label in Ala$_{10}$ is not close enough to a ^{15}N to contribute to ΔS. A completely unambiguous determination of the carbonyl-carbon resonance frequency of [1-^{13}C]Ala$_{17}$ as 177 ppm is made using eight rotor cycles of REDOR dipolar evolution (Fig. 3). In this situation, only ^{13}C labels with a strong, one-bond ^{13}C-^{15}N coupling have resonances appearing in the difference spectrum. The only carbonyl ^{13}C in the labeled K3 peptide that fits this description is the labeled carbonyl carbon of Ala$_{17}$. The upfield shoulder of the 177 ppm peak in the full-echo spectra is not present in the REDOR difference spectra and is assigned to the lipid carbonyls.

The carbonyl-carbon resonance frequency of [1-^{13}C]Ala$_{10}$ also occurs at 177 ppm (Fig. 4, *top*). This signal was selected by a 16-rotor cycle CEDRA experiment (Zhu et al., 1994). Just as in the REDOR experiment, for short dipolar evolution times, only ^{13}C-^{13}C pairs separated by one or two bonds contribute to the difference spectrum and the 177-ppm peak is dominated by the ^{13}C-labeled pair of Ala$_{10}$-Gly$_{11}$. The 45-ppm peak in the difference spectrum arises primarily from the methylene ^{13}C label in Gly$_{11}$. However, there is currently not enough information in the literature about the chemical shift of the α-carbon in glycine to use this shift in secondary structure determination.

The observed chemical shifts from Figs. 2–4 (and from measurements made on lyophilized and fully hydrated samples with an L/P = 20) are presented in Table 1, along with literature values for solid-state chemical shifts typical of α-helix and β-sheet conformations. The isotropic ^{13}C chemical shifts from the three labeled clusters of (KIAG-KIA)$_3$-NH$_2$ are only consistent with a single α-helical

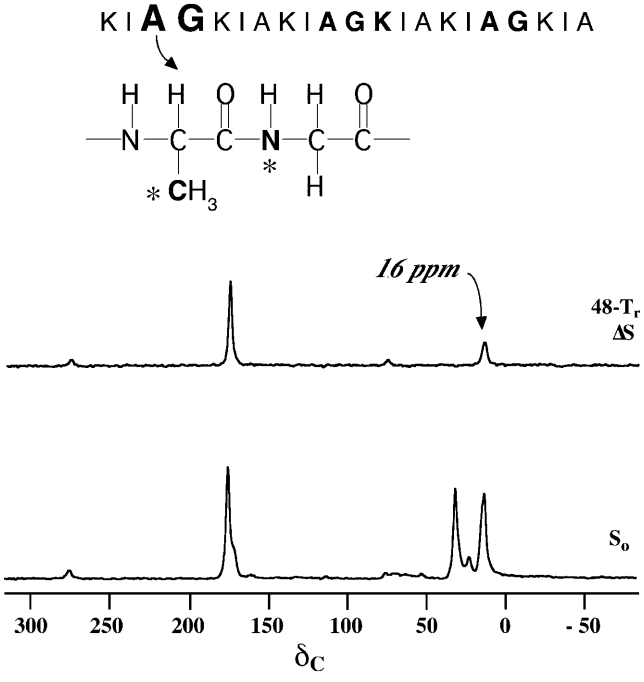

FIGURE 2 50.3-MHz REDOR $^{13}C\{^{15}N\}$ NMR spectra of [3-^{13}C]Ala$_3$-[^{15}N]Gly$_4$-[1-^{13}C]Ala$_{10}$-[2-^{13}C]Gly$_{11}$-[6-^{15}N]Lys$_{12}$-[1-^{13}C]Ala$_{17}$-[^{15}N]Gly$_{18}$-(KIAGKIA)$_3$-NH$_2$ incorporated into MLVs of DPPG and DPPC (1:1) at a lipid/peptide molar ratio of 10, after 48 rotor cycles of dipolar evolution with MAS at 5000 Hz. The full-echo spectrum (S_o) is shown at the bottom of the figure and the REDOR difference spectrum (ΔS, the difference between the ^{13}C echo intensities observed without and with ^{15}N dephasing pulses) at the top.

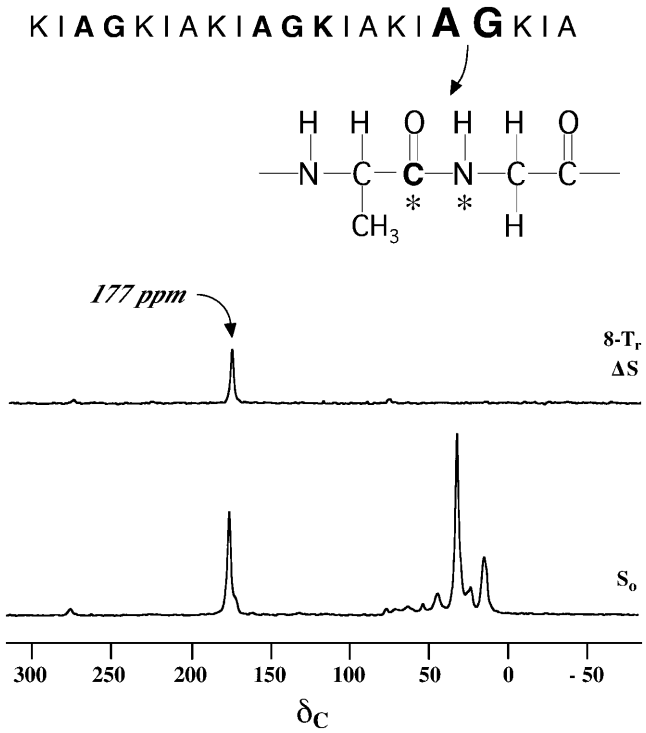

FIGURE 3 50.3-MHz REDOR $^{13}C\{^{15}N\}$ NMR spectra of the sample of Fig. 2 after eight rotor cycles of dipolar evolution with MAS at 5000 Hz.

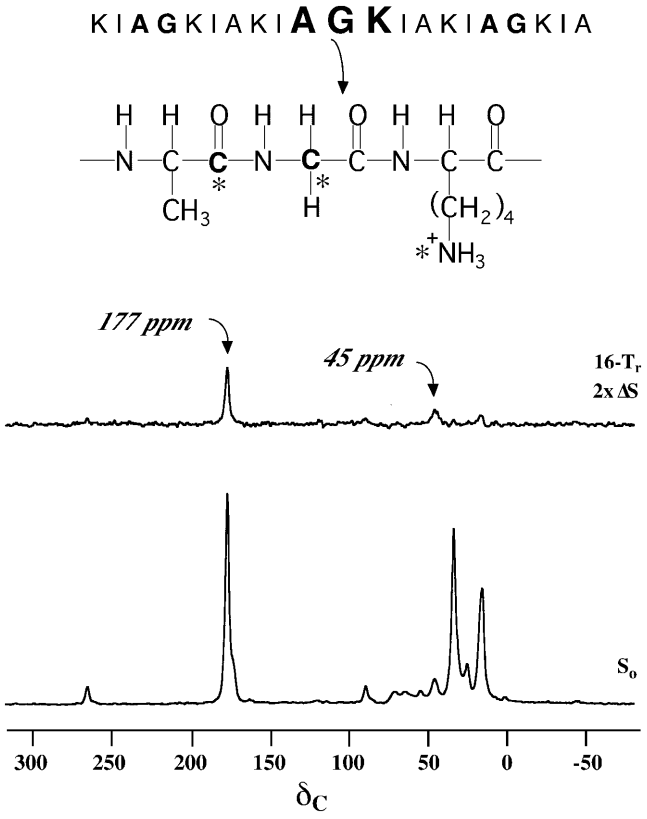

FIGURE 4 50.3-MHz CEDRA ^{13}C NMR spectra of the sample of [3-^{13}C]Ala$_3$-[^{15}N]Gly$_4$-[1-^{13}C]Ala$_{10}$-[2-^{13}C]Gly$_{11}$-[6-^{15}N]Lys$_{12}$-[1-^{13}C]Ala$_{17}$-[^{15}N]Gly$_{18}$-(KIAGKIA)$_3$-NH$_2$ incorporated into MLVs of DPPG and DPPC (1:1) at a lipid/peptide molar ratio of 10, after 16 rotor cycles of dipolar evolution with MAS at 4427 Hz. This spinning speed is two-thirds of the separation of the centerband frequencies of the methylene ^{13}C label in Gly$_{11}$ and the carbonyl ^{13}C label in Ala$_{10}$, a choice that results in optimum refocusing for the determination of S_o.

conformation for the entire peptide chain in the phospholipid bilayer. There are no β-sheet or random-coil chemical shifts. The REDOR and CEDRA recoupling methods used for spectral editing would have allowed the detection of as little as 2% β-sheet conformation.

Bilayer lipid phases with and without K3

Nonspinning ^{31}P NMR experiments were carried out on lyophilized and hydrated MLVs of pure lipids (DPPG/DPPC, 1:1), as well as on MLVs in the presence of K3 at L/P = 20. The observed ^{31}P NMR spectra (Fig. 5) show the characteristic lineshapes of organized lipid bilayers in both cases (Smith and Eikel, 1984). In the case of the lyophilized samples (Fig. 5, *a* and *b*), a powder pattern characteristic of a static phosphodiester moiety appears in both the absence and the presence of the peptide. For the hydrated samples (Fig. 5, *c* and *d*), a shape reminiscent of the static powder pattern appears at temperatures below −30°C, where large-amplitude motion is largely suppressed. Small-amplitude motion is still present, as evidenced by the blurring of the sharper features of the powder pattern. Increasing the temperature results in a gradual narrowing of the line and the appearance of an axially symmetric powder pattern that arises from the rapid axial rotation of the phosphodiester moiety. The presence of the peptide has virtually no effect on the width of the spectrum, which is ~175 ppm at −10°C and 75 ppm at +10°C. The absence of narrow, isotropic resonances proves that large lamellar structures are preserved even in the presence of the peptide at L/P = 20. The shape of the pattern at +10°C excludes the possibility of an inverted hexagonal (H_{II}) lipid phase (Smith and Eikel, 1984).

TABLE 1 Solid-state NMR ^{13}C chemical shifts (ppm from tetramethylsilane) of carbonyl and methyl carbons for alanine in various secondary structures

	α-Helix*	β-Sheet*	Lyophilized†,‡	Hydrated†,§
[1-^{13}C]Ala	176.4	171.8	177	177
[3-^{13}C]Ala	15.1	20.1	16	16

*Saito (1986).
†‡This work, for K3 in a sugar-protected lipid matrix at lipid/peptide molar ratios of 10, 20, and 40.
†§This work, for K3 in a frozen, fully hydrated bilayer at a lipid/peptide molar ratio of 20.

Peptide-lipid headgroup contact

$^{13}C\{^{31}P\}$ REDOR

Fig. 6 shows the ^{13}C full-echo (S_o, *solid lines*) and ^{31}P dephased (S, *dotted lines*) spectra of the carbonyl region of [3-^{13}C]Ala$_3$-[^{15}N]Gly$_4$-[1-^{13}C]Ala$_{10}$-[2-^{13}C]Gly$_{11}$-[6-^{15}N]Lys$_{12}$-[1-^{13}C]Ala$_{17}$-[^{15}N]Gly$_{18}$-K3 incorporated into MLVs of DPPC/DPPG (1:1) at L/P = 20. The spectra were obtained after 64 rotor cycles of dipolar evolution from MLVs in a sugar-protected lyophilized state (*left*) and in a frozen, fully hydrated state (*right*). The peak at 177 ppm arises from ^{13}C carbonyl labels at Ala$_{10}$ and Ala$_{17}$ as well as natural-abundance carbonyl ^{13}C in the peptide. The sizeable dephasing indicates the proximity of the peptide chain to the phosphorous headgroups in the lipid bilayer in both samples. The upfield peak at 173 ppm is from natural abundance ^{13}C carbonyls in the lipid headgroups. Dephasing of this peak arises mainly from strong intramolecular ^{13}C-^{31}P contacts in the phospholipids with a small intermolecular contribution between neighboring lipid headgroups. We attribute the somewhat diminished dephasing of both peaks in the hydrated sample to motional averaging of dipolar couplings.

The $^{13}C\{^{31}P\}$ REDOR spectra of the lyophilized sample after 96 rotor cycles of dipolar evolution at a MAS speed of 5000 Hz is shown in Fig. 7. In addition to the peaks in the carbonyl region discussed above, the peak in the ΔS spectrum at 16.1 ppm is attributed to the ^{13}C methyl label in Ala$_3$. This REDOR difference indicates contact between the N-terminal region of the peptide and the lipid headgroups.

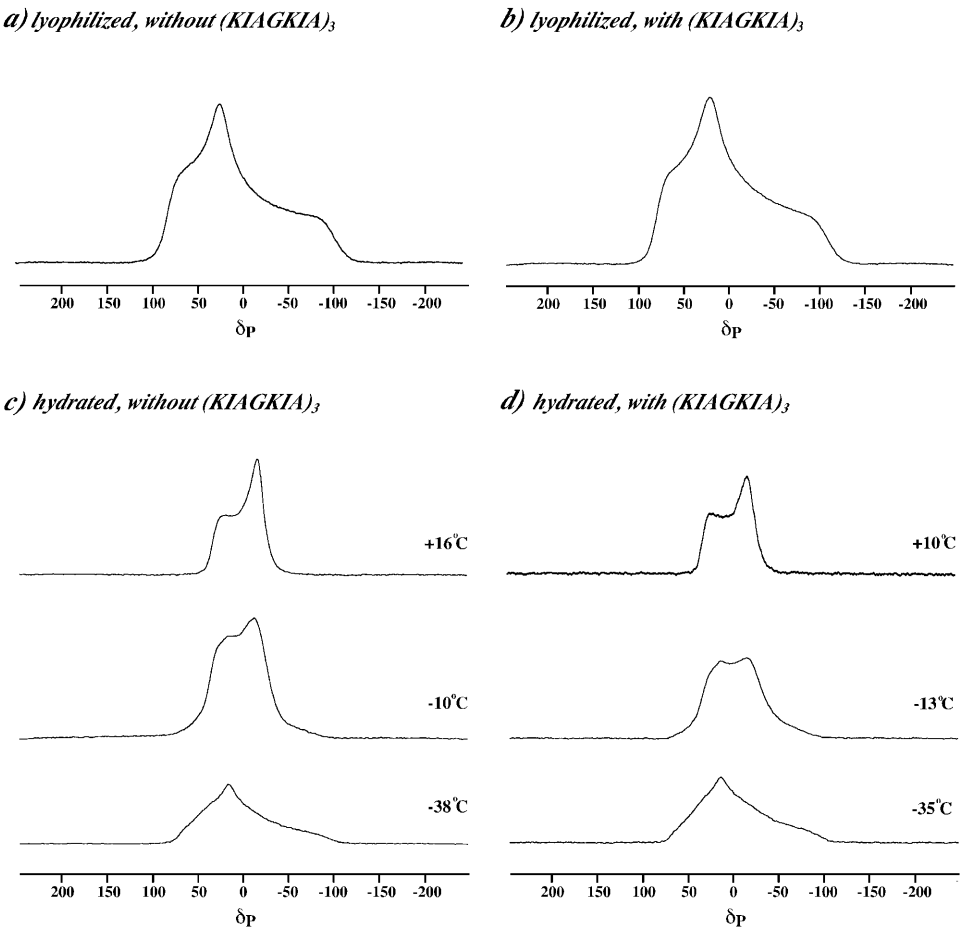

FIGURE 5 Static 81-MHz ^{31}P NMR spectra of synthetic MLVs of DPPC/DPPG (1:1) in the absence (*left*) and in the presence (*right*) of $(KIAGKIA)_3$-NH_2; lyophilized (*top*) and frozen, fully hydrated (*bottom*) state. Spectra have been scaled with respect to sample mass and the number of scans.

Fig. 8 shows the observed carbonyl-carbon $^{13}C\{^{31}P\}$ dephasing ($\Delta S/S_o$) for [1-^{13}C]Ala_{10}-[^{15}N]Gly_{11}-K3 as a function of dipolar evolution time for L/P = 10 (*open circles*), 20 (*solid circles*), and 40 (*open squares*). This version of K3 was used to avoid any ambiguity in the position of the ^{13}C. Although this label might be in the vicinity of several phosphorous headgroups, a short ^{13}C-^{31}P separation of ~5–6 Å seems to dominate. The analysis of the $\Delta S/S_o$ (*solid lines*) in terms of a single nearest-neighbor dephaser suggests an average internuclear ^{13}C-^{31}P separation of 5.9 Å for L/P = 10, 5.5 Å for L/P = 20, and 4.8 Å for L/P = 40; that is, the proximity of labels to the phosphate decreases slightly for increasing peptide concentration. At the same time, the fraction of peptide chains with detectable ^{13}C-^{31}P contact

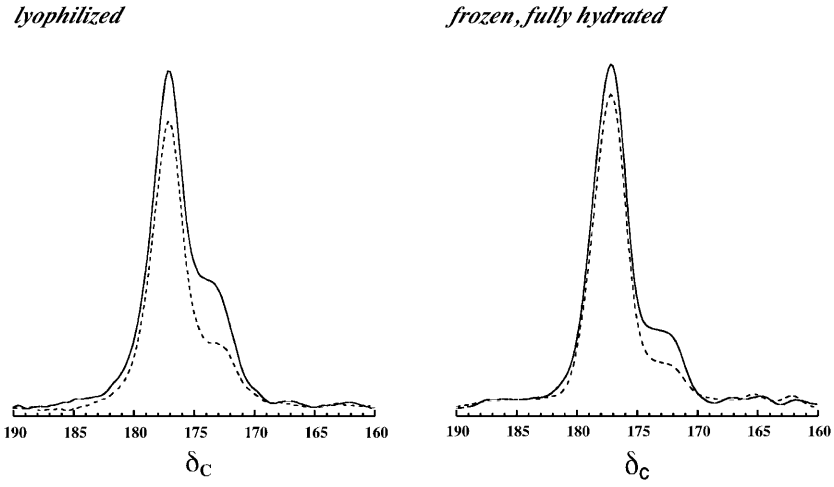

FIGURE 6 Carbonyl regions of 50.3-MHz $^{13}C\{^{31}P\}$ REDOR S_o (*solid lines*) and S (*dotted lines*) spectra of [3-^{13}C]Ala_3-[^{15}N]Gly_4-[1-^{13}C]Ala_{10}-[2-^{13}C]Gly_{11}-[6-^{15}N]Lys_{12}-[1-^{13}C]Ala_{17}-[^{15}N]Gly_{18}-$(KIAGKIA)_3$-NH_2, incorporated into synthetic MLVs of DPPG/DPPC (1:1) at a lipid/peptide molar ratio of 20. The spectra were obtained after 64 rotor cycles of dipolar evolution with MAS at 5000 Hz with the MLVs in a sugar-protected lyophilized state (*left*) and in a frozen, fully hydrated state (*right*). The upfield peak (173 ppm) is from the phospholipid headgroups and is ~50% dephased after a dipolar evolution time of 12.8 ms. The downfield peak (177 ppm) arises from the ^{13}C carbonyl labels at Ala_{10} and Ala_{17}, as well as natural abundance ^{13}C carbonyl (~9% of the signal), in the peptide chains. The temperature was ~−10°C for the lyophilized sample and −25°C for the hydrated sample.

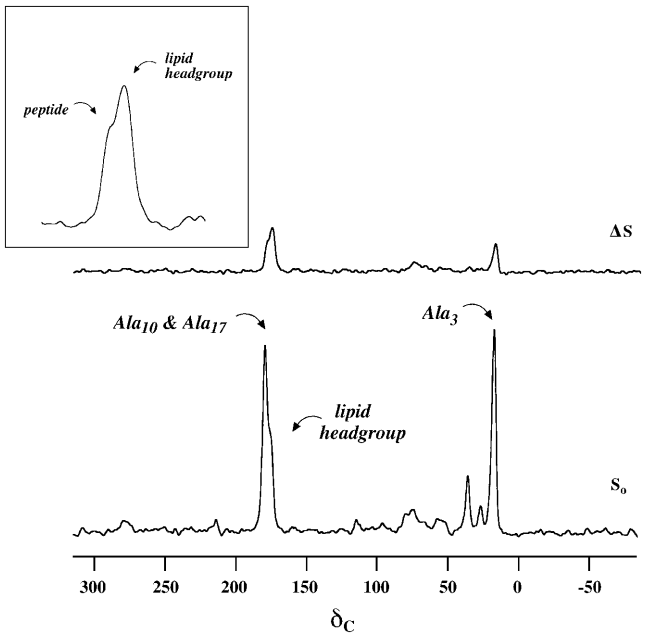

FIGURE 7 50.3-MHz $^{13}C\{^{31}P\}$ REDOR full-echo (S_o) and difference (ΔS) spectra of [3-^{13}C]Ala$_3$-[^{15}N]Gly$_4$-[1-^{13}C]Ala$_{10}$-[2-^{13}C]Gly$_{11}$-[6-^{15}N]Lys$_{12}$-[1-^{13}C]Ala$_{17}$-[^{15}N]Gly$_{18}$-(KIAGKIA)$_3$-NH$_2$, incorporated into synthetic MLVs of DPPG/DPPC (1:1) at a lipid/peptide molar ratio of 20 after 96 rotor cycles of dipolar evolution with MAS at 5000 Hz. The C_α of Gly has a short T_2 relaxation and therefore is not observed in the spectrum after 96 rotor cycles. An expansion of the 175-ppm region of the difference spectrum is shown in the inset. The sample was lyophilized and the experimental temperature was ~ -10°C.

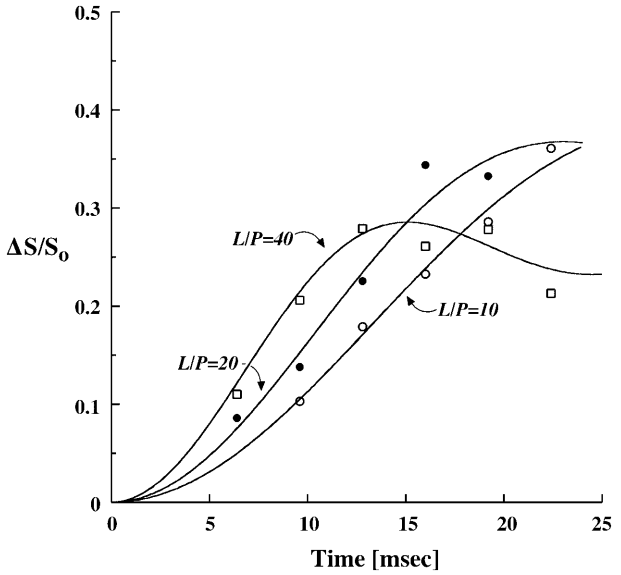

FIGURE 8 50.3-MHz $^{13}C\{^{31}P\}$ REDOR dephasing ($\Delta S/S_o$) for the peptide carbonyl magnetization of a 50-50 mixture of [1-^{13}C]Ala$_{10}$-[^{15}N]Gly$_{11}$- and [2-^{2}H, 3-^{19}F]Ala$_{10}$-(KIAGKIA)$_3$-NH$_2$ in MLVs of DPPG/DPPC (1:1) at a lipid/peptide molar ratio of 10 (○), 20 (●), and 40 (□). MAS was at 5000 Hz. All samples were lyophilized in a protecting sugar matrix. The solid lines are best fits to the experimental $\Delta S/S_o$ values and correspond to a mean internuclear ^{13}C-^{31}P separation of 5.9 Å (L/P = 10), 5.5 Å (L/P = 20), and 4.8 Å (L/P = 40). The distribution widths were in the range of 0.2–0.4 Å. The carbonyl region of both the S_o and the S (or ΔS) spectra was deconvoluted for the analysis.

increases from 25% for L/P = 40 to 35% for L/P =10 and 20.

$^{15}N\{^{31}P\}$ REDOR

To gain insight into the relative positions of the lysine side chains with respect to the phospholipid headgroups, $^{15}N\{^{31}P\}$ REDOR experiments were performed on [3-^{13}C]Ala$_3$-[^{15}N]Gly$_4$-[1-^{13}C]Ala$_{10}$-[2-^{13}C]Gly$_{11}$-[6-^{15}N]Lys$_{12}$-[1-^{13}C]Ala$_{17}$-[^{15}N]Gly$_{18}$-K3 in MLVs of DPPG/DPPC (1:1) at L/P = 20. Fig. 9 shows the REDOR difference and full echo spectra after 128 rotor cycles of ^{31}P dephasing. The peak at 79 ppm is assigned to the two labeled backbone amide nitrogens (Gly$_4$ and Gly$_{18}$), whereas the peak at 8.6 ppm is from the labeled amine nitrogen of Lys$_{12}$. Both peaks dephase substantially. The dephasing of the peak at 79 ppm arises from the interaction of the backbone nitrogens at Gly$_4$ and possibly Gly$_{18}$ (suggested by $^{13}C\{^{19}F\}$ REDOR results, see below) with the phosphorous in the lipid headgroups. The $\Delta S/S_o$ value of 0.56 measured for the lysine side-chain nitrogen indicates the proximity of the side chain to the lipid headgroups. The dephasing corresponds to an ''apparent'' ^{15}N-^{31}P distance of 5.2 Å. However, the REDOR difference signal of the lysine nitrogen is asymmetric, suggesting two populations of peptide chains in two, slightly different chemical environments: one with a tighter and the other one with a somewhat looser [6-^{15}N]Lys$_{12}$-^{31}P contact.

Peptide-lipid tail contact

$^{13}C\{^{19}F\}$ REDOR experiments on MLVs containing phospholipids with a single ^{19}F label at the end of one of their fatty acid acyl chains (Fig. 10) were carried out to determine which parts of the peptide chains are in contact with phospholipid tails. The fluorinated phospholipid content of the vesicles was 2.5 mol %. At this level of F-lipid incorporation, the fluorines do not significantly perturb the bilayer structure (McDonough et al., 1983). To confirm this conclusion, K3-induced dye-leakage experiments were carried out on small unilamellar vesicles of DPPG/DPPC (1:1) with and without fluorinated-lipid incorporation in the same concentration range that was used in the NMR experiments. The behavior of the fluorinated-lipid vesicles was virtually indistinguishable from that of the nonfluorinated vesicles (see Fig. 11 of II).

The full-echo (S_o) and difference (ΔS) $^{13}C\{^{19}F\}$ REDOR spectra of [3-^{13}C]Ala$_3$-[^{15}N]Gly$_4$-[1-^{13}C]Ala$_{10}$-[2-^{13}C]Gly$_{11}$-[6-^{15}N]Lys$_{12}$-[1-^{13}C]Ala$_{17}$-[^{15}N]Gly$_{18}$-K3 in MLVs of DPPG/F-DPPG/DPPC/F-DPPC (48.75:1.25:48.75:1.25) at L/P = 20 are shown after 48 rotor cycles of dipolar evolution at a MAS speed of 5000 Hz in Fig. 11. The peak in

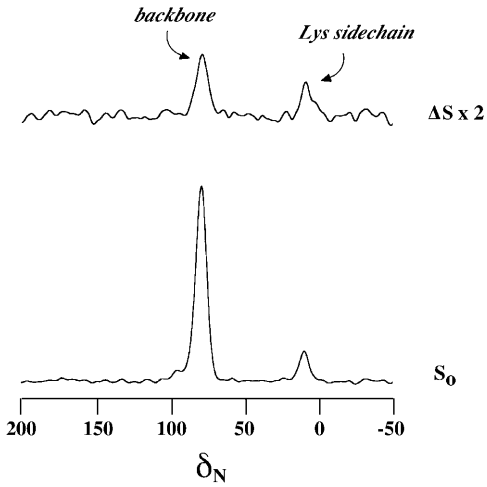

FIGURE 9 20.3-MHz $^{15}N\{^{31}P\}$ REDOR full-echo (S_o) and difference (ΔS) spectra of [3-^{13}C]Ala$_3$-[^{15}N]Gly$_4$-[1-^{13}C]Ala$_{10}$-[2-^{13}C]Gly$_{11}$-[6-^{15}N]Lys$_{12}$-[1-^{13}C]Ala$_{17}$-[^{15}N]Gly$_{18}$-(KIAGKIA)$_3$-NH$_2$, incorporated into synthetic MLVs of DPPG/DPPC (1:1) at a lipid/peptide molar ratio of 20, after 128 rotor cycles of dipolar evolution with MAS at 5000 Hz. The sample was lyophilized in a protecting trehalose matrix. The experimental temperature was ~ -10°C.

the ΔS spectrum at 177 ppm indicates the proximity of the carbonyl carbon at Ala$_{10}$ and/or at Ala$_{17}$ to the fluorinated lipid tails. There appears to be minor dephasing at 16 ppm that may arise from contacts between lipid chains and the ^{13}C methyl label at Ala$_3$. Its small size suggests that the N-terminal end of the peptide chains is somewhat farther away from the lipid tails than is the C-terminal end.

The dependence of $\Delta S/S_o$ at 177 ppm on the dephasing time is shown in Fig. 12. The dephasing matches that expected for an isolated ^{13}C-^{19}F pair with an average internuclear separation of 7.7 Å and a distribution width of 3.6 Å. The $\Delta S/S_o$ plateaus at $\sim$36%, indicating that one in every three carbonyl-carbon labels is in contact with a fluorinated lipid tail. This is a large number for a fluorinated lipid concentration of only 2.5%, which suggests that the carboxyl terminal half of the peptide chains (Ala$_{10}$-Ala$_{17}$) is near a large number of lipid tails. In fact, the plateau of $\Delta S/S_o$ at 36% indicates that $\sim$28 lipid tails (14 lipid molecules, .36/.025 $\approx$ 14) are within 12 Å of the Ala$_{10}$-Ala$_{17}$ region of the peptide chain.

Lipid headgroup-lipid tail contact

The $^{31}P\{^{19}F\}$ REDOR spectra of lyophilized and hydrated MLVs of DPPG/DPPC (1:1) with either 2.5 mol % or 5.0 mol % F-DPPG/F-DPPC (1:1) (see Fig. 10) are shown in Fig. 13. The peaks in the REDOR difference spectra (ΔS) (Fig. 13, *top*) after 80 rotor cycles of ^{19}F dephasing arise from lipid headgroups that experience observable dipolar couplings to the fluorines in the terminal-CH_2F groups of the lipid acyl chains. Dephasing is most likely the result of both intra- and intermolecular ^{31}P-^{19}F couplings. Increasing the fluorine concentration by a factor of two for the hydrated sample relative to that for the lyophilized sample results in approximately twice as much dephasing (Fig. 13, *bottom*). This result indicates similar strengths of the ^{31}P-^{19}F dipolar coupling in the two samples. Thus, large-amplitude motional averaging of the interaction in the hydrated sample has been suppressed by freezing, and headgroup-tail contact is not an artifact of lyophilization.

Enhanced lipid headgroup-lipid tail contact in the presence of K3

Fig. 14 shows the $^{31}P\{^{19}F\}$ dephasing for MLVs of DPPG/DPPC (1:1) (2.5 mol % F-lipid included) with and without peptide incorporation. Incorporation of the peptide results in

F-DPPC

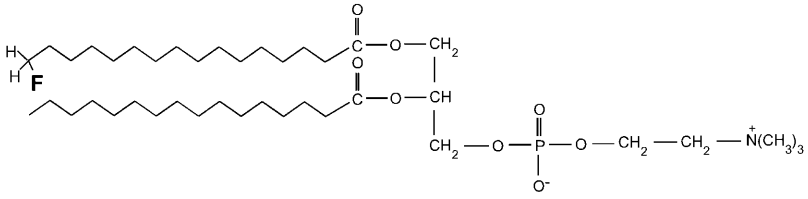

F-DPPG

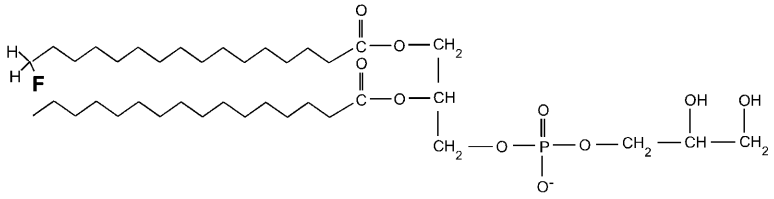

FIGURE 10 Chemical structures of 1-palmitoyl-2-[16-fluoropalmitoyl]-phosphatidylcholine (F-DPPC) and 1-palmitoyl-2-[16-fluoropalmitoyl]-phosphatidylglycerol (F-DPPG). The fluorine labels are shown in bold.

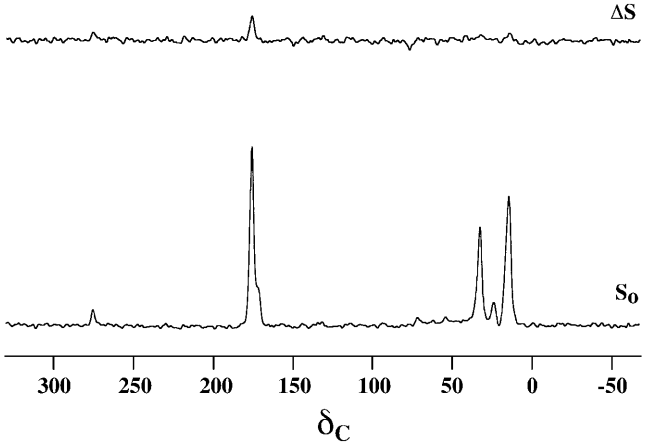

FIGURE 11 50.3-MHz $^{13}C\{^{19}F\}$ REDOR full-echo (S_o) and difference (ΔS) spectra of [3-^{13}C]Ala$_3$-[^{15}N]Gly$_4$-[1-^{13}C]Ala$_{10}$-[2-^{13}C]Gly$_{11}$-[6-^{15}N]Lys$_{12}$-[1-^{13}C]Ala$_{17}$-[^{15}N]Gly$_{18}$-(KIAGKIA)$_3$-NH$_2$ in MLVs of DPPC/F-DPPC/DPPG/F-DPPG (48.75:1.25:48.75:1.25) at a lipid/peptide molar ratio of 20, after 48 rotor cycles of dipolar evolution with MAS at 5000 Hz. The sample was lyophilized in a protecting trehalose matrix. The C_α peak of glycine has a short T_2 relaxation time and therefore is not observable in the spectrum after 48 rotor cycles.

an increase in headgroup-tail contact in the bilayer. Two conclusions can be made immediately: i), the larger initial slope of the $\Delta S/S_o$ dephasing as a function of evolution time in the presence of the peptide indicates a shorter average P-F

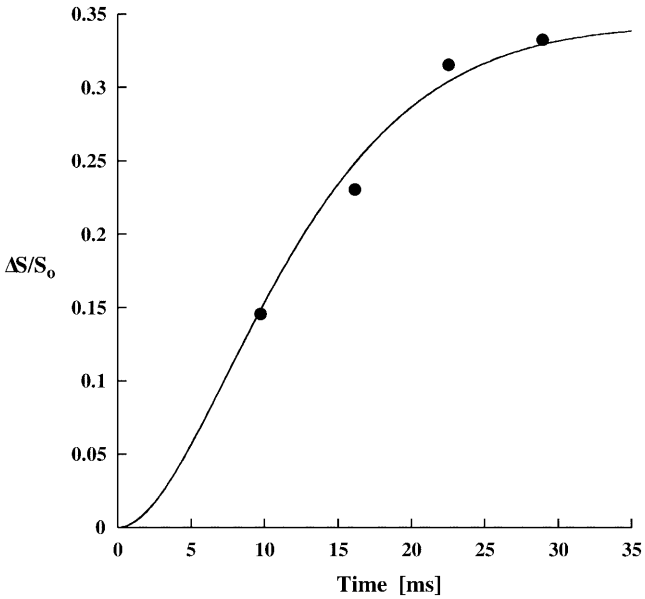

FIGURE 12 50.3-MHz $^{13}C\{^{19}F\}$ REDOR dephasing ($\Delta S/S_o$) of the carbonyl magnetization of [3-^{13}C]Ala$_3$-[^{15}N]Gly$_4$-[1-^{13}C]Ala$_{10}$-[2-^{13}C]Gly$_{11}$-[6-^{15}N]Lys$_{12}$-[1-^{13}C]Ala$_{17}$-[^{15}N]Gly$_{18}$-(KIAGKIA)$_3$-NH$_2$ in MLVs of DPPC/F-DPPC/DPPG/F-DPPG (48.75:1.25:48.75:1.25) at a lipid/peptide molar ratio of 20. The sample was lyophilized in a protecting trehalose matrix. The solid line drawn through the experimental points corresponds to a distribution of isolated ^{13}C-^{19}F spin pairs with a mean internuclear separation of 7.7 Å and a distribution width of 3.6 Å.

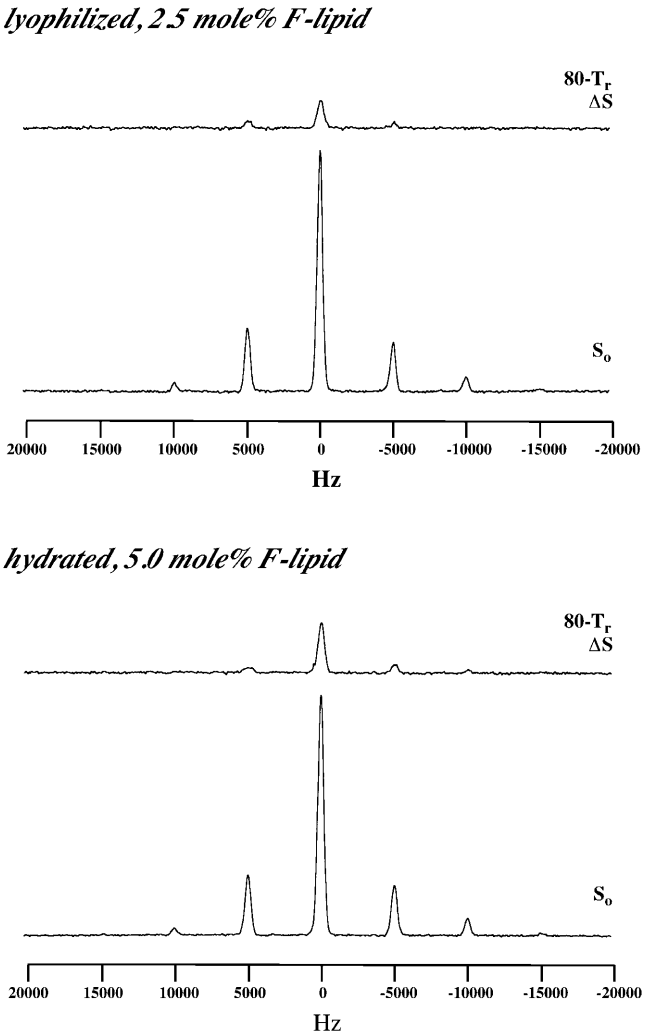

FIGURE 13 81-MHz $^{31}P\{^{19}F\}$ REDOR spectra of synthetic MLVs of DPPC/DPPG (1:1). (*Top*) Lyophilized sample in the presence of 2.5 mol % F-DPPC/F-DPPG. (*Bottom*) Frozen, fully hydrated sample in the presence of 5.0 mol % F-DPPC/F-DPPG. Both sets of spectra were acquired after 80 rotor cycles of dipolar evolution with MAS at 5000 Hz. The spectra resulted from the accumulation of 34,128 scans in the lyophilized state and 61,616 scans in the frozen, fully hydrated state. The spectra are scaled so that the full-echo centerbands are the same height. The experimental temperature was ~ -10°C for the lyophilized sample and -25°C for the hydrated sample.

distance; and ii), the higher plateau suggests that a larger fraction of headgroups are in proximity to the lipid tails when the peptide is incorporated into the membrane. In more quantitative terms, the dephasing in the absence of the peptide fits well to a model in which ~22% of the phosphorous atoms are coupled to a fluorine with a mean internuclear ^{31}P-^{19}F separation of 9.9 Å and a distribution width of 1.6 Å. In the presence of the peptide, ~33% of the phosphorous atoms are in proximity to lipid tails, and the mean internuclear ^{31}P-^{19}F separation decreases to 7.6 Å with a distribution width of 5.4 Å. The wider distribution of shorter P-F distances (Fig. 15) is an indication of an

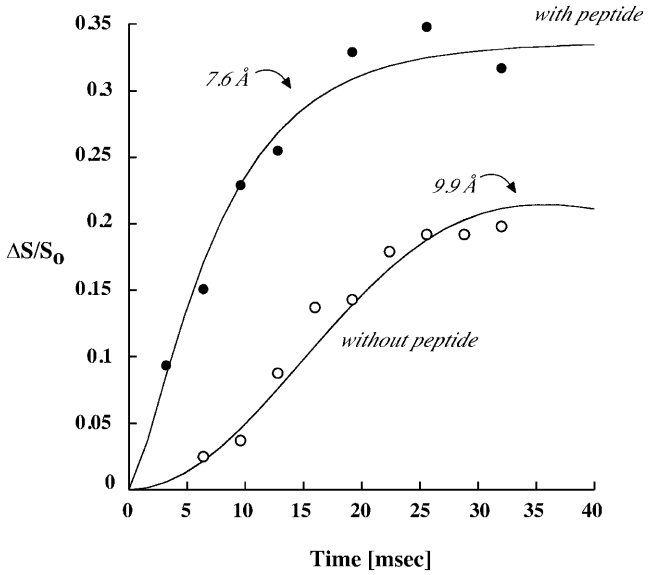

FIGURE 14 81-MHz $^{31}P\{^{19}F\}$ REDOR dephasing ($\Delta S/S_o$) of DPPG/F-DPPG/DPPC/F-DPPC (48.75:1.25:48.75:1.25) MLVs in the presence (●) and in the absence (○) of [3-^{13}C]Ala$_3$-[^{15}N]Gly$_4$-[1-^{13}C]Ala$_{10}$-[2-^{13}C]Gly$_{11}$-[6-^{15}N]Lys$_{12}$-[1-^{13}C]Ala$_{17}$-[^{15}N]Gly$_{18}$-(KIAGKIA)$_3$-NH$_2$ at a lipid/peptide molar ratio of 20. Both samples were lyophilized in a protecting sugar matrix. The solid lines drawn through the experimental points are simulated dephasing curves assuming a distribution of isolated ^{31}P-^{19}F spin pairs with a mean internuclear separation of 7.6 Å and a distribution width of 5.4 Å (●), or a mean internuclear separation of 9.9 Å with a distribution width of 1.6 Å (○).

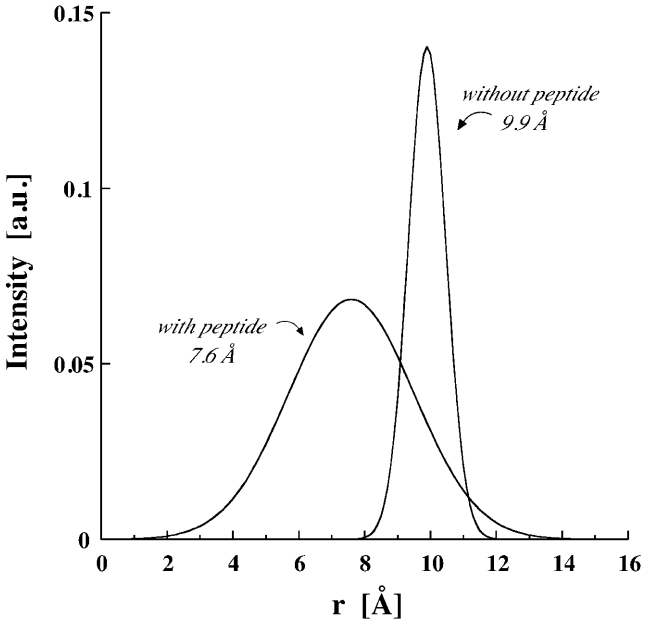

FIGURE 15 Distribution of ^{31}P-^{19}F distances in the presence and in the absence of (KIAGKIA)$_3$-NH$_2$ in MLVs of DPPG/DPPC (1:1) at 2.5 mol % of fluorinated lipid (F-DPPG/F-DPPC, 1:1) incorporation.

increased disorder among the lipid molecules when K3 is incorporated.

DISCUSSION

Secondary structure

The use of site-specific labeling makes possible the determination of peptide conformation at the single-residue level. By employing three clusters of ^{13}C and ^{15}N labels along the sequence of K3 (one at the beginning, one in the middle, and one at the end of the peptide chain), the combination of REDOR with chemical-shift information shows that the entire peptide is in an α-helical conformation in the phospholipid bilayer at lipid/peptide molar ratios of 10, 20, and 40. No β-sheet or random-coil conformation is observed. The recoupling methods used for spectral editing would have allowed the detection of as little as 2% β-sheet conformation. This result is consistent with a recent investigation of K3 in the presence of large unilamellar vesicles of anionic phospholipids by circular dichroism spectroscopy in the solution state (Blazyk et al., 2001). Due to the repetitive sequence of (KIAGKIA)$_3$-NH$_2$, the peptide forms an α-helix with a narrow positively charged wedge (~60°), whereas the rest of the cross section of the helix is hydrophobic. The fact that the entire (KIAGKIA)$_3$-NH$_2$ chain forms an α-helix suggests that the whole molecule is embedded in the bilayer so that the backbone as well as the hydrophobic face of the molecule are in contact with the lipid acyl chains.

Qualitative features of lipid morphology

Differential scanning calorimetry and leakage studies indicate that helical peptides that are able to mimic the shape of certain types of phospholipids can either stabilize or destabilize the structure of lipid bilayers (Epand et al., 1995). The latter can lead to the formation of inverted lipid phases (Tytler et al., 1993). The room-temperature, static ^{31}P lineshapes of Fig. 5 exclude the possibility of the formation of an inverted hexagonal phase in the presence of K3 for both frozen hydrated and lyophilized systems. These results are consistent with the finding that both magainin 2 and PGLa, K3 analogs that are the two major antimicrobial peptides from *Xenopus laevis,* induce positive curvature strain on lipid bilayers (Wieprecht et al., 1997). Furthermore, the absence of narrow, isotropic resonances in the ^{31}P NMR spectra of Fig. 5 proves that large lamellar structures are preserved even in the presence of the peptide at L/P = 20. This means that except for pore formation, the MLVs are intact.

Blazyk and et al. (2001) recently found that K3 had a negligible effect on the bilayer-to-hexagonal phase transition temperature of 1,2-dipalmitoleoylphosphatidylethanolamine (DiPoPE), a phospholipid with a tendency to form structures with a negative curvature. The reason for this seeming anomaly is most likely the difference in the lipid composition of the two systems. The double bond in the

middle of the acyl chains in DiPoPE results in highly kinked lipid chains that can perhaps better accommodate the peptide chains within the bilayer. In addition, in the absence of acidic phospholipids, the peptide-bilayer interaction is expected to be much weaker in DiPoPE than in DPPC/DPPG (1:1).

Peptide-lipid headgroup contact

The $^{15}N\{^{31}P\}$ REDOR experiments of Fig. 9 show direct structural evidence of the proximity of the Lys_{12} side chain of K3 to the phosphodiester moieties, consistent with strong electrostatic interactions between the ε-amino group of lysines and the acidic lipid headgroups. The ability of the long, amphipathic lysine side chains to maintain favorable electrostatic interactions with negatively charged lipid headgroups, while at the same time allowing the peptide backbone to penetrate deeply into the hydrophobic membrane core, is well documented in the literature and is often referred to as the ''snorkel model'' (Segrest et al., 1990).

The $^{13}C\{^{31}P\}$ REDOR experiments on Ala_{10}- and $Ala_{17}(^{13}C{=}O)$-labeled K3 chains (Fig. 6) indicate proximity of K3 to lipid headgroups at L/P = 20 for both lyophilized and frozen fully hydrated MLVs. The contact is therefore not an artifact of the lyophilization. With labels in both the middle and end of K3, this result is consistent with any of the three models of Fig. 1. The $^{13}C\{^{31}P\}$ REDOR experiments on the $Ala_{10}(^{13}C{=}O)$-labeled K3 of Fig. 8 have provided additional evidence of peptide-headgroup contact. In this case the ^{13}C label is just in the middle of the K3 chain. Regardless of peptide concentration (in the range of lipid/peptide molar ratios of 10–40), an internuclear ^{13}C-^{31}P separation of 5–6 Å was observed for ~30% of the carbonyl carbons of Ala_{10}. Since Ala_{10} is two residues away from Lys_{12}, it is located on the opposite side of the helix. Therefore it is not surprising that only $\sim 1/3$ of the peptide chains are oriented so that the carbonyl carbon at Ala_{10} is also near a phosphorous. The ''phosphorous-proximate'' population increases slightly with increasing peptide concentrations (25% at L/P = 40 and 35% at L/P = 20 and 10), which is most likely explained by an increasingly crowded interfacial area in the bilayer. The sizeable dephasing of the ^{13}C magnetization in Ala_{10}, and the fact that there is an increase in dephasing rather than a decrease with increasing peptide concentration, are not consistent with a barrel-stave pore model (Ehrenstein and Lecar, 1977). This model would position the labeled carbonyl in Ala_{10} approximately at the midpoint of the bilayer (Fig. 1 *A*), which would give rise to dephasing more than an order of magnitude smaller than observed.

Peptide-lipid tail contact

The substantial $^{13}C\{^{19}F\}$ dephasing of Fig. 11 means that a large number of $Ala_{10}(^{13}C{=}O)$-, $Ala_{17}(^{13}C{=}O)$-labeled K3 chains have contact with the fluorinated lipid tails despite the low ^{19}F incorporation in the tails of the lipid acyl chains (2.5%). The lesser dephasing for the methyl ^{13}C label at Ala_3 suggests that the N-terminal of the peptide chains is perhaps tightly anchored to the headgroup region. The extra positive charge at the amino-end may play a role in preventing a deeper penetration. The extensive ^{13}C-^{19}F contact in the Ala_{10}-Ala_{17} region correlates with the biological observation that K3 chains amidated at their C-terminus show increased activity. Amidated chains are likely to penetrate more deeply into the hydrophobic acyl chain region than their charged counterparts. The fact that ~36% of the K3 chains had detectable ^{19}F dephasing in the region of Ala_{10}-Ala_{17} suggests that the majority of peptide chains are surrounded by ~14 lipid molecules.

The extensive peptide-lipid tail contact detected by $^{13}C\{^{19}F\}$ correlates with the $^{31}P\{^{19}F\}$ REDOR results for ^{19}F-labeled MLVs of DPPG/DPPC (1:1) that have shown an enhanced contact between lipid headgroups and lipid tails in the presence of K3 at L/P = 20 (Fig. 14; cf. below). In addition, the similarity of P-F dipolar couplings measured in lyophilized and frozen fully hydrated samples indicates that headgroup-tail contact is not an artifact of lyophilization. Nevertheless, quantitative details of the lipid structure (such as the exact number of lipid tails in contact with peptide chains cited above) observed in lyophilized MLVs should be confirmed using fully hydrated samples.

Lipid headgroup-lipid tail contact

The $^{31}P\{^{19}F\}$ REDOR results of Fig. 14 indicate that qualitatively there is enhanced contact between the phospholipid headgroups and the tails of the lipid acyl chains, resulting from the presence of K3, at L/P = 20. (A similar contact has been observed by $^{13}C\{^{31}P\}$ REDOR for the natural-abundance lipid methyl carbon of DPPC-DPPG MLVs.) This is in the concentration range where magainin-like peptides (Ludtke et al., 1994, 1996) as well as K3 (see II) were found to reorient with respect to the membrane normal, and where dye leakage has been observed for both magainin peptides (Matsuzaki, 1998a,b) and K3 (Blazyk et al., 2001). One way to account for the increased headgroup-tail contact is that the peptide induces partial interdigitation among the phospholipids. Interdigitation has been observed for a variety of amphipathic structures (Rowe, 1985; Cunningham et al., 1989; Rowe and Cutrera, 1990) that accumulate at the interfacial region of the bilayer.

Another possibly more likely explanation for the headgroup-tail contact is that the presence of the peptide induces the lipid tails to bend back toward the headgroups. This distortion of the lipid acyl chains would fill the energetically highly unfavorable gaps that the peptide chains create upon partitioning into the bilayer. The importance of membrane flexibility, as evidenced by the diminished activity of magainin-like peptides in the presence of cholesterol (Matsuzaki et al., 1995) supports this hypothesis. To a certain

extent, headgroup-tail contact appears to exist even in the absence of the peptide, as evidenced by REDOR for frozen fully hydrated MLVs (Fig. 13, *bottom*), and several other techniques for fully hydrated systems near physiological temperatures (Feller et al., 1999; Huster et al., 1999). Both interdigitation and enhanced headgroup-tail contact by bending would be consistent with the observation that antimicrobial peptides such as magainin cause a thinning in the lipid bilayer (Ludtke et al., 1996).

This work was supported by National Institutes of Health grant EB02058 (J.S.).

REFERENCES

Andreu, D., and L. Rivas. 1998. Animal antimicrobial peptides: an overview. *Biopolymers.* 47:415–433.

Bechinger, B., M. Zasloff, and S. J. Opella. 1993. Structure and orientation of the antibiotic peptide magainin in membranes by solid-state NMR spectroscopy. *Protein Sci.* 2:2077–2084.

Blazyk, J., R. Wiegand, J. Klein, J. Hammer, R. M. Epand, R. F. Epand, W. L. Maloy, and U. P. Kari. 2001. A novel linear amphipathic β-sheet cationic antimicrobial peptide with enhanced selectivity for bacterial lipids. *J. Biol. Chem.* 276:27899–27906.

Bowman, H. G., J. Marsh, and J. A. Goode. 1994. Antimicrobial peptides. *Ciba Foundation Symposium, 186*. John Wiley & Sons, Chichester, UK. 1–272.

Crowe, J. H., and L. M. Crowe. 1984. Preservation of membranes in anhydrobiotic organisms: the role of trehalose. *Science.* 223:701–704.

Cunningham, B. A., W. Tamura-Lis, L. J. Lis, and J. M. Collins. 1989. Thermodynamic properties of acyl chain and mesophase transitions for phospholipids in KSCN. *Biochim. Biophys. Acta.* 984:109–112.

Esfahani, M., J. R. Cavanaugh, P. E. Pfeffer, D. W. Luken, and T. M. Devlin. 1981. ^{19}F-NMR and fluorescence polarization of yeast plasma membrane and isolated lipids. *Biochem. Biophys. Res. Comm.* 101:306–311.

Ehrenstein, G., and H. Lecar. 1977. Electrically gated ionic channels in lipid bilayers. *Q. Rev. Biophys.* 10:1–34.

Epand, R. M., Y. Shai, J. P. Segrest, and G. M. Anantharamaiah. 1995. Mechanisms for the modulation of membrane bilayer properties by amphipathic helical peptides. *Biopolymers.* 37:319–338.

Epand, R. M., and H. J. Vogel. 1999. Diversity of antimicrobial peptides and their mechanisms of action. *Biochim. Biophys. Acta.* 1462:11–28.

Feller, S. E., D. Huster, and K. Gawrisch. 1999. Interpretation of NOESY cross-relaxation rates from molecular dynamics simulation of a lipid bilayer. *J. Am. Chem. Soc.* 121:8963–8964.

Gullion, T., D. B. Baker, and M. S. Conradi. 1990. New, compensated Carr-Purcell sequences. *J. Magn. Res.* 89:479–484.

Gullion, T., and J. Schaefer. 1989a. Rotational echo double-resonance NMR. *J. Magn. Reson.* 81:196–200.

Gullion, T., and J. Schaefer. 1989b. Detection of weak heteronuclear dipolar coupling by rotational-echo double resonance. *Adv. Magn. Reson.* 13:57–83.

Hancock, R. E. W., and G. Diamond. 2000. The role of cationic antimicrobial peptides in innate host defenses. *Trends Microbiol.* 8:402–410.

Hing, A. W., S. Vega, and J. Schaefer. 1992. Transferred-echo double-resonance NMR. *J. Magn. Reson.* 96:205–209.

Hirsh, D. J., J. Hammer, W. L. Maloy, J. Blazyk, and J. Schaefer. 1996. Secondary structure and location of a magainin analog in synthetic phospholipid bilayers. *Biochemistry.* 35:12733–12741.

Huang, H. W. 2000. Action of antimicrobial peptides: two-state model. *Biochemistry.* 39:8347–8352.

Huster, D. and K. Gawrisch. 2000. New insights into biomembrane structure from two-dimensional nuclear Overhauser enhancement spectroscopy. *In* Lipid Bilayers: Structure and Interactions. J. Katsaras and T. Gutberlet, editors. Springer, Berlin. 109–126.

Kates, M. 1986. Techniques of lipidology: isolation, analysis and identification of lipids, 2nd revised ed. *In* Laboratory Techniques in Biochemistry. R. H. Burdon and P. H. Knippenberg, editors. Elsevier, Amsterdam and New York. 114–115.

Ludtke, S. J., K. He, W. T. Heller, T. A. Harroun, L. Yang, and H. W. Huang. 1996. Membrane pores induced by magainin. *Biochemistry.* 33:13723–13728.

Ludtke, S. J., K. He, Y. Wu, and H. W. Huang. 1994. Cooperative membrane insertion of magainin correlated with its cytolytic activity. *Biochim. Biophys. Acta.* 1190:181–184.

Maloy, L. M., and U. P. Kari. 1995. Structure-activity studies on magainins and other host defense peptides. *Biopolymers.* 37:105–122.

Matsuzaki, K., D. Chapman, and P. Haris. 1998a. Biomembrane Structures. IOS Press, Amsterdam. 205–227.

Matsuzaki, K. 1998b. Magainins as paradigm for the mode of action of pore forming polypeptides. *Biochim. Biophys. Acta.* 1376:391–400.

Matsuzaki, K., K.-I. Sugishita, N. Fujii, and K. Miyajima. 1995. Molecular basis for membrane selectivity of an antimicrobial peptide, magainin 2, in phospholipid bilayers. *Biochemistry.* 34:3423–3429.

McDonough, B., P. M. Macdonald, B. D. Sykes, and R. N. McElhaney. 1983. Fluorine-19 nuclear magnetic resonance studies of lipid fatty acyl chain order and dynamics in *Acholeplasma laidlawaii B* membranes. A physical, biochemical, and biological evaluation of monofluoropalmitic acids as membrane probes. *Biochemistry.* 22:5097–5103.

Mueller, K. T. 1995. Analytic solutions for the time evolution of dipolar-dephasing NMR signal. *J. Magn. Reson. Series A.* 113:81–93.

O'Connor, R. D., and J. Schaefer. 2002. Relative CSA-dipolar orientation from REDOR sidebands. *J. Magn. Reson.* 154:46–52.

O'Connor, R. D., B. Poliks, D. H. Bolton, J. M. Goetz, J. A. Byers, K. L. Wooley, and J. Schaefer. 2002. Chain-packing in linear phenol-polycarbonate by $^{13}C\{^{2}H\}$ REDOR. *Macromolecules.* 35:2608–2617.

Pouny, Y., D. Rapaport, A. Mor, P. Nicolas, and Y. Shai. 1992. Interaction of antimicrobial dermaseptin and its fluorescently labeled analogues with phospholipid membranes. *Biochemistry.* 31:12416–12423.

Rowe, E. S. 1985. Thermodynamic reversibility of phase transitions. Specific effects of alcohols on phosphatidylcholines. *Biochim. Biophys. Acta.* 813:321–330.

Rowe, E. S., and T. A. Cutrera. 1990. Differential scanning calorimetric studies of ethanol interactions with distearoylphosphatidylcholine: transition to the interdigitated phase. *Biochemistry.* 29:10398–10404.

Rudolph, A. S., and J. J. Crowe. 1985. Membrane stabilization during freezing: the role of two natural cryoprotectants, trehalose and proline. *Cryobiology.* 22:367–377.

Saitô, H. 1986. Conformation-dependent ^{13}C chemical shifts: a new means of conformational characterization as obtained by high-resolution solid-state ^{13}C NMR. *Magn. Reson. Chem.* 24:835–852.

Segrest, J. P., H. De Loof, J. G. Dohlman, C. G. Brouillettem, and G. M. Anantharamaiah. 1990. Amphipathic helix motif: classes and properties. *Proteins.* 8:103–117.

Shai, Y. 1999. Mechanisms of the binding, insertion and destabilization of phospholipid bilayer membranes by α-helical antimicrobial and cell non-selective membrane-lytic peptides. *Biochim. Biophys. Acta.* 1462:55–70.

Smith, I. C. P., and I. H. Eikel. 1984. Phosphorous-31 NMR of phospholipids in membranes. *In* Phosphorous-31 NMR Principles and Applications. Academic Press.

Soravia, E., G. Martini, and M. Zasloff. 1988. Antimicrobial properties of peptides from *Xenopus* granular gland secretions. *FEBS Lett.* 228:337–340.

Tytler, E. M., J. P. Segrest, R. M. Epand, S.-Q. Nie, R. F. Epand, V. K. Mishra, Y. V. Venkatachalapathi, and G. M. Anantharamaiah. 1993. Reciprocal effects of apolipoprotein and lytic peptide analogs on membranes. *J. Biol. Chem.* 268:22112–22118.

Van't Hof, W., E. C. Veerman, E. J. Helmerhorst, and A. V. N. Amerongenm. 2001. Antimicrobial peptides: properties and applicability. *Biol. Chem.* 382:597–619.

Wieprecht, T., M. Dathe, R. M. Epand, M. Beyermann, E. Krause, W. L. Maloy, D. L. MacDonald, and M. Bienert. 1997. Influence of the angle subtended by the positively charged helix face on the membrane activity of amphipathic, antibacterial peptides. *Biochemistry.* 36:12869–12880.

Zasloff, M. 1987. Magainins, a class of antimicrobial peptides from *Xenopus* skin: isolation, characterization of two active forms, and partial cDNA sequence of a precursor. *Proc. Natl. Acad. Sci. USA.* 84:5449–5453.

Zhu, W., C. A. Klug, and J. Schaefer. 1994. Measurement of dipolar coupling within isolated spin-1/2 homonuclear pairs by CEDRA NMR. *J. Magn. Reson.* 108:121–123.